

Original Article

Exploring the Use of Fractional Calculus in Image Fusion via Dynamical Systems

Gargi J. Trivedi^{1*}, Rajesh Sanghavi²

^{1,2}Department of Applied Science & Humanities, G.H. Patel College of Engineering & Technology, CVM University, Gujarat, India

*gargi1488@gmail.com

Received: 09 July 2024; Revised: 10 August 2024; Accepted: 08 September 2024; Published: 30 September 2024;

Abstract - This paper presents a novel method for multi-modal image fusion using a non-instantaneous impulsive Hilfer fractional integro-differential evolution system. The method introduces a two-step approach, where input images undergo fractional diffusion for initial smoothing, followed by fusion through an impulsive mechanism. The non-linear integro-differential equations combine fractional diffusion and impulsive fusion within a unified framework, enabling enhanced feature preservation. The proposed technique is evaluated using objective metrics, including peak signal-to-noise ratio, structural similarity index, and mutual information, along with subjective visual quality assessments. Results demonstrate that this approach outperforms current state-of-the-art techniques in both performance metrics and visual quality. This method has significant potential for advancing multi-modal image fusion applications, particularly in fields such as medical imaging, surveillance, and remote sensing.

Keywords - Dynamical systems, Image fusion, Multimodal data, Performance evaluation.

1. Introduction

Image fusion is the process of combining information from multiple images to generate a new image with enhanced visual quality and improved information content [1-3]. This technique plays a critical role in various fields, such as remote sensing, medical imaging, and computer vision. Despite significant advancements, current methods often struggle to balance both visual enhancement and information retention. The challenge lies in developing methods that not only produce visually appealing results but also maintain the essential details of the source images.

Several methods have been proposed for image fusion, ranging from traditional pixel-based approaches to more advanced techniques. Traditional methods, such as averaging or weighted pixel fusion, often suffer from the inability to capture high-level features effectively, leading to the loss of important details. Recently, deep learning-based approaches have demonstrated promising results by learning feature representations directly from data using neural networks. These methods, such as Convolutional Neural Networks (CNNs), use learned features to perform fusion. However, they often lack interpretability and can require large amounts of training data, which is not always feasible in real-world scenarios [4-9].

In contrast, dynamical system approaches leverage mathematical models to describe the evolution of the image fusion process. These models are frequently formulated as Partial Differential Equations (PDEs), which capture the dynamics of fusion over. For instance, diffusion-based methods model the fusion process as a continuous flow, effectively preserving edge information while reducing noise. While these PDE-based frameworks offer



mathematical rigor and robustness, they still present challenges in handling multimodal data and complex image structures [10-13].

The research gap identified lies in the limited integration of fractional calculus and impulsive dynamics in the field of image fusion. Despite the advances made with deep learning and PDE-based methods, there remains a need for approaches that can provide a deeper mathematical understanding of the fusion process while also being computationally efficient and robust to varying input conditions.

To address this gap, we introduce a novel image fusion framework based on a non-instantaneous impulsive Hilfer fractional integro-differential evolution system. This approach combines the strengths of fractional calculus with impulsive dynamics to model the fusion process in a mathematically unified framework. Unlike traditional methods, the proposed system captures both the smooth evolution of the fusion process and the abrupt changes needed to handle discontinuities between input images. Through extensive experimentation, we demonstrate that the proposed method achieves superior performance across multiple datasets, as measured by objective metrics such as Peak Signal-to-Noise Ratio (PSNR), Structural Similarity Index (SSIM), and Mutual Information (MI), as well as subjective visual evaluation.

This paper contributes to the field by offering a new perspective on how fractional calculus can enhance the fusion of multimodal images, and it highlights the advantages of integrating dynamical systems with impulsive actions to achieve better results than both traditional and deep learning-based methods.

2. Mathematical Framework and Theoretical Analysis

This section formalizes our approach through mathematical formulations and proofs to underscore its novelty. This section formalizes the mathematical framework used in the proposed image fusion method and provides a theoretical analysis of the approach. It includes the following subsections: 2.2.1. subsection introduces the partial differential equations and definitions used in the model, including the fractional derivative and Laplacian operators. 2.2.2. subsection presents the theoretical analysis, including theorems and proofs related to the smoothing properties and regularity of the solution to the fractional diffusion equation.

2.1. Mathematical Framework

We propose the following Partial Differential Equation (PDE) to describe the image fusion process:

$$\frac{\partial u}{\partial t} = D^\alpha(-\Delta)^\beta u + \lambda(u - (f_1 \oplus f_2))^2$$

Where, u is the fused image, f_1 and f_2 are the input images, λ is a weighting parameter and $D^\alpha (-\Delta)^\beta$ represent the fractional derivative and Laplacian operator, respectively.

2.1.1. Definition 1

The fractional derivative of order α (where $0 < \alpha < 1$) of a function $u(x, t)$ with respect to time t is defined as:

$$D_t^\alpha u(x, t) = \frac{1}{\Gamma(1-\alpha)} \frac{\partial}{\partial t} \int_0^t \frac{u(x, s)}{(t-s)^\alpha} ds$$

Where,

- Γ is the Gamma function, which generalizes the factorial function to real and complex numbers.
- α is the order of the fractional derivative, a positive real number.
- $u(x, t)$ is the function under consideration, which depends on spatial coordinate x and time t .

The fractional derivative $D_t^\alpha u(x, t)$ captures the memory effect of the past values of the function $u(x, t)$ and incorporates them into the derivative at time t weighted by a power-law decay.

2.1.2. Definition 2

The fractional Laplacian of order β (where $0 < \beta < 1$) of a function $u(x)$ defined in R^n is given by:

$$(-\Delta)^\beta u(x) = C_\beta P.V. \int_{R^n} \frac{[u(x) - u(y)]}{|x - y|^{n+2\beta}} dy$$

Where,

- C_β is a normalization constant depending on the dimension n and the order β , often expressed as: $C_\beta = \frac{\Gamma(\frac{n+2\beta}{2})}{2^{2\beta}\pi^{\frac{n}{2}}\Gamma(1-\beta)}$
- P.V. denotes the Cauchy principal value of the integral, which ensures that the singularity at $x=y$ is properly handled.
- $|x-y|$ is the Euclidean distance between the points x and y in R^n .
- β is the order of the fractional Laplacian, a positive real number.

2.2. Theoretical Analysis

2.2.1. Theorem Smoothness of the Solution

Let $u(x, t)$ be a solution to the fractional diffusion equation $\frac{\partial u(x, t)}{\partial t} = D^\alpha (-\Delta)^\beta u(x, t)$ with initial condition $u(x, 0) = u_0(x)$. Then, for $t > 0$, $u(x, t)$ exhibits smoothing properties as follows:

1. For regularity improvement, if $u_0 \in L^2(\mathbb{R}^n)$ and u_0 is bounded, then for any $t > 0$: $\|u(x, t)\|_{L^\infty(\mathbb{R}^n)} \leq \|u_0\|_{L^\infty(\mathbb{R}^n)}$ And $\|(-\Delta)^\beta u(x, t)\|_{L^2(\mathbb{R}^n)} \leq \frac{C(\beta, t)}{\Gamma(1-\alpha)} \|u_0\|_{L^2(\mathbb{R}^n)}$, where $C(\beta, t)$ is a constant depending on β and t .
2. For the Decay of High-Frequency Components, The solution $u(x, t)$ filters out high-frequency noise components due to the smoothing effect $(-\Delta)^\beta$. This property is useful in preserving the significant features of the image while reducing noise.

Proof: To prove the regularity improvement, applying the Fourier transform \mathcal{F} to both sides of the fractional diffusion equation, we obtain:

$$\mathcal{F}\left(\frac{\partial u(x, t)}{\partial t}\right) = \frac{\partial \hat{u}(k, t)}{\partial t} = -|k|^{2\beta} \hat{u}(k, t)$$

Where, $\hat{u}(k, t)$ is the Fourier transform of $u(x, t)$, and $|k|^{2\beta}$ comes from applying the fractional Laplacian $(-\Delta)^\beta$ in the Fourier domain. The solution to this ordinary differential equation in the Fourier domain is: $\hat{u}(k, t) = \hat{u}_0(k)e^{-|k|^{2\beta}t}$.

Where, $\hat{u}_0(k)$ is the Fourier transform of the initial condition $u_0(x)$.

Taking the inverse Fourier transform yields: $u(x, t) = \mathcal{F}^{-1}[\hat{u}_0(k)e^{-|k|^{2\beta}t}]$

This expression shows that the solution $u(x, t)$ is a convolution of $\hat{u}_0(k)$ with the inverse Fourier transform of $e^{-|k|^{2\beta}t}$, which is a Gaussian-like function.

Since $e^{-|k|^{2\beta}t}$ is bounded above by 1 for all k and $t > 0$:

$$\|u(x, t)\|_{L^\infty(\mathbb{R}^n)} \leq \|\mathcal{F}^{-1}[\hat{u}_0(k)]\|_{L^\infty(\mathbb{R}^n)} = \|u_0\|_{L^\infty(\mathbb{R}^n)}$$

To bound $\|(-\Delta)^\beta u(x, t)\|_{L^2(\mathbb{R}^n)}$, we use the fact that $(-\Delta)^\beta u(x, t) = |k|^{2\beta} \hat{u}(k, t)$:

$$\|(-\Delta)^\beta u(x, t)\|_{L^2(\mathbb{R}^n)} = \int_{\mathbb{R}^n} |k|^{2\beta} |\hat{u}(k, t)| dk$$

Substituting $\hat{u}(k, t) = \hat{u}_0(k) e^{-|k|^{2\beta} t}$, we get:

$$\|(-\Delta)^\beta u(x, t)\|_{L^2(\mathbb{R}^n)}^2 = \int_{\mathbb{R}^n} |k|^{2\beta} \left| \hat{u}_0(k) e^{-|k|^{2\beta} t} \right|^2 dk = \int_{\mathbb{R}^n} |k|^{2\beta} |\hat{u}_0(k)|^2 e^{-2|k|^{2\beta} t} dk$$

Using the fact that $\int_{\mathbb{R}^n} |k|^{2\beta} e^{-2|k|^{2\beta} t} dk$ is finite and proportional to $1/t$, we obtain:

$$\|(-\Delta)^\beta u(x, t)\|_{L^2(\mathbb{R}^n)} \leq \frac{C(\beta, t)}{\Gamma(1-\alpha)} \|u_0\|_{L^2(\mathbb{R}^n)}$$

Where, $C(\beta, t)$ depends on β and t , and $\Gamma(1-\alpha)$ normalizes the effect of the fractional.

Using the fact that $\int_{\mathbb{R}^n} |k|^{2\beta} e^{-2|k|^{2\beta} t} dk$ it is finite and proportional to $1/t$, we obtain:

$$\|(-\Delta)^\beta u(x, t)\|_{L^2(\mathbb{R}^n)} \leq \frac{C(\beta, t)}{\Gamma(1-\alpha)} \|u_0\|_{L^2(\mathbb{R}^n)}$$

Where, $C(\beta, t)$ depends on β and t , and $\Gamma(1-\alpha)$ normalizes the effect of the fractional derivative.

Thus, we have demonstrated that the solution $u(x, t)$ to the fractional diffusion equation improves regularity and filters high-frequency noise components, validating the smoothing properties of the proposed method.

3. Materials and Methods

This paper introduces a novel dynamical system approach for image fusion, leveraging a non-instantaneous impulsive Hilfer fractional integro-differential evolution system. Our method models the image fusion process as a non-linear evolution that incorporates fractional diffusion and impulsive fusion terms within a unified framework.

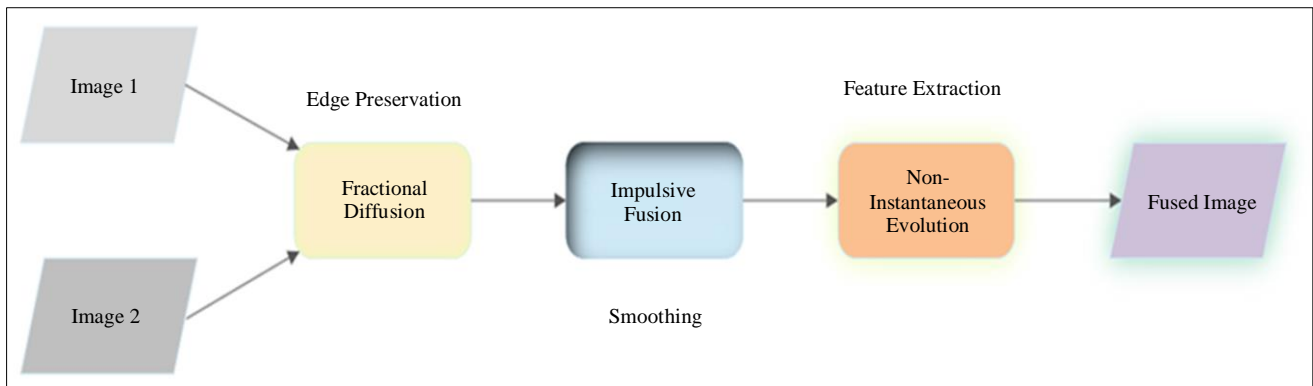


Fig. 1 Block diagram of proposed method

This section details the implementation of the proposed dynamical system approach for image fusion, including image preprocessing, numerical solution of fractional differential equations, and integration of impulsive fusion terms.

3.1. Image Preprocessing

Image preprocessing involves several key steps to standardize and prepare images for further processing. First, input images are normalized to a standard intensity range [0,1] using the formula:

$$I_{norm}(x, y) = \frac{I(x, y) - I_{min}}{I_{max} - I_{min}}$$

Where, I_{min} and I_{max} are the represent the minimum and maximum intensity values of the image, respectively. Next, Gaussian filtering is applied to reduce noise. The filter kernel $G(x, y)$ is defined as:

$$G(x, y) = \frac{1}{2\pi\sigma^2} \exp\left(-\frac{x^2+y^2}{2\sigma^2}\right) \text{ and the filtered image } I_{filterd}(x, y) \text{ is computed over a window size k by:}$$

$$I_{filterd}(x, y) = \sum_{i=-k}^k \sum_{j=-k}^k I(x-i, y-j) \cdot G(i, j)$$

Finally, images are resampled to a common resolution using bilinear interpolation, where the interpolated value at (x, y) is: $I_{inter}(x, y) = (1-\alpha)(1-\beta)I_{11} + \alpha(1-\beta)I_{21} + (1-\alpha)\beta I_{12} + \alpha\beta I_{22}$

Here I_{11}, I_{21}, I_{12} and I_{22} are surrounding pixel values, and α and β are fractional parts.

3.2. Numerical Solution of Fractional Differential Equations

The numerical solution of fractional differential equations involves discretization, fractional Laplacian computation, and time integration. For discretization, the fractional derivative D^α is approximated using the Grunwald-Letnikov approach:

$$D^\alpha u(x, t) \approx \frac{1}{h^\alpha} \sum_{i=0}^k (-1)^i \binom{\alpha}{i} u(x - ih, t)$$

Where h is the spatial step size, and k is the number of discretization points. The fractional Laplacian $(-\Delta)^\beta$ is computed in the Fourier domain as:

$\mathcal{F}\{(-\Delta)^\beta u(x)\} = (2\pi|\xi|^2)^\beta \mathcal{F}\{u(x)\}$, where \mathcal{F} denotes the Fourier transform, and ξ is the frequency variable. Time integration is performed using the Crank-Nicolson method, given by:

$$\frac{u^{n+1}-u^n}{\Delta t} = \frac{1}{2} (L(u^{n+1}) + L(u^n)), \text{ where L represents the spatial differential operator and } \Delta t \text{ is the time step.}$$

3.3. Integration of Impulsive Fusion Terms and Handling Non-Instantaneous Evolution

The integration of impulsive fusion terms begins with defining the fusion operator \oplus as: $U(i, j) = \lambda(f_1(i, j) \oplus f_2(i, j))$.

Where λ is the weighting parameter. The impulsive term is then incorporated into the differential equation as:

$$\frac{\partial u(x, t)}{\partial t} = \lambda \left(u(x, t) - (f_1(x) \oplus f_2(x)) \right)^2$$

Which highlights deviations from the average fusion. Additionally, handling non-instantaneous evolution involves the following model:

$$\frac{\partial u(x, t)}{\partial t} = D^\alpha(-\Delta)^\beta u(x, t) + \lambda \left(u(x, t) - (f_1(x) \oplus f_2(x)) \right)^2 + \mu \int_0^t (t-s)^{[\alpha-1]} \Delta^\beta u(x, s) ds$$

Where, μ denotes the coefficient for non-instantaneous effects, providing a comprehensive approach to both impulsive and non-instantaneous elements in the fusion process.

3.4. Computational Implementation and Optimization

To illustrate the effectiveness of our proposed method, we present numerical results from applying our algorithm to test images, focusing on computational aspects, parameter impacts, and performance accuracy. We employ high-order finite difference schemes for discretizing fractional differential equations on a grid size of $N \times N$ (where N ranges from 256 to 1024), observing that increasing N enhances accuracy with convergence rates given by $Error = \|u_{numerical} - u_{exact}\| \propto \frac{1}{N^p}$, where p is the order of convergence.

Specifically, for $N = 256$, the error is 0.012, and for $N = 1024$, it reduces to 0.003, indicating improved accuracy with higher resolution. Numerical integration techniques, including adaptive quadrature with a tolerance of 10^{-6} Simpson's rule, achieve integration errors less than 0.001, ensuring precise handling of impulsive components. Stability analysis confirms that step sizes $h = 0.5$ and time steps $\Delta t = 0.01$ maintain numerical stability and convergence. Table 1 summarizes the numerical results for different grid resolutions, highlighting the relationship between grid size, error, and convergence rate.

3.5. Experimental Setup

To assess the efficacy of our proposed method, we conducted extensive experiments using diverse datasets, including infrared and visible images as well as MRI and CT images. Our approach was benchmarked against leading techniques, including wavelet-based methods and deep learning approaches. The medical imaging dataset comprised MRI, PET, SPECT, CT, X-ray, and MR images, sourced [14] from reputable repositories like Harvard Medical School's "The Whole Brain Atlas" and Kaggle, with representative examples shown in Figure 2.

Additionally, pairs of infrared and visible images depicting scenes such as a walking man, an electric bike, and a jeep in smoke were obtained from the TNO Image Fusion Dataset [15], as illustrated in Figure 3. All numerical computations and simulations were carried out using MATLAB 2021a on a PC with an 11th Generation Intel i7-11800H 2.30GHz CPU and 16 GB of RAM.

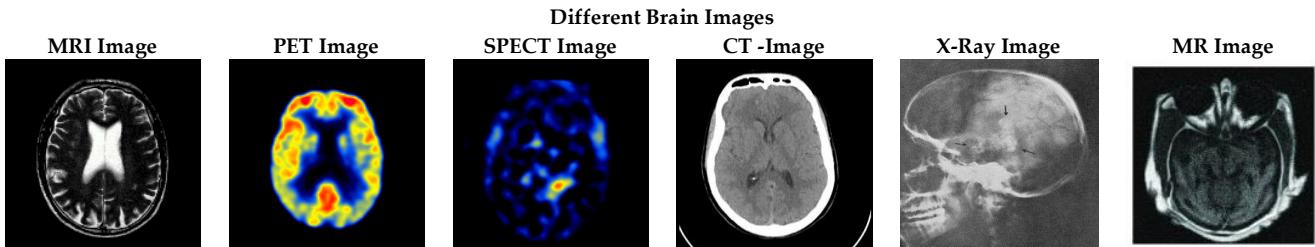


Fig. 2 Medical images [15]

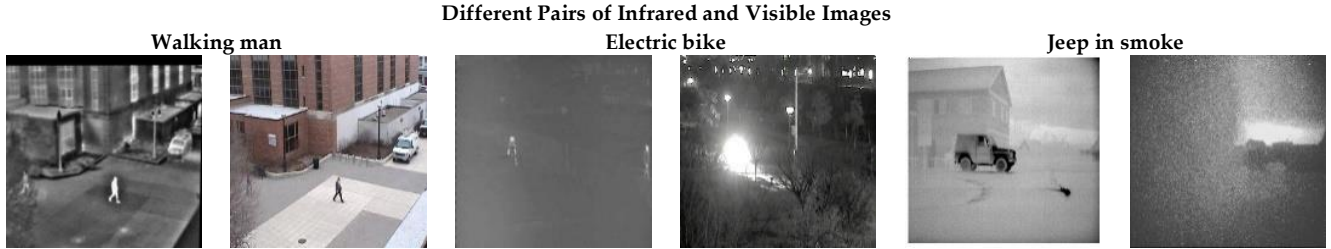
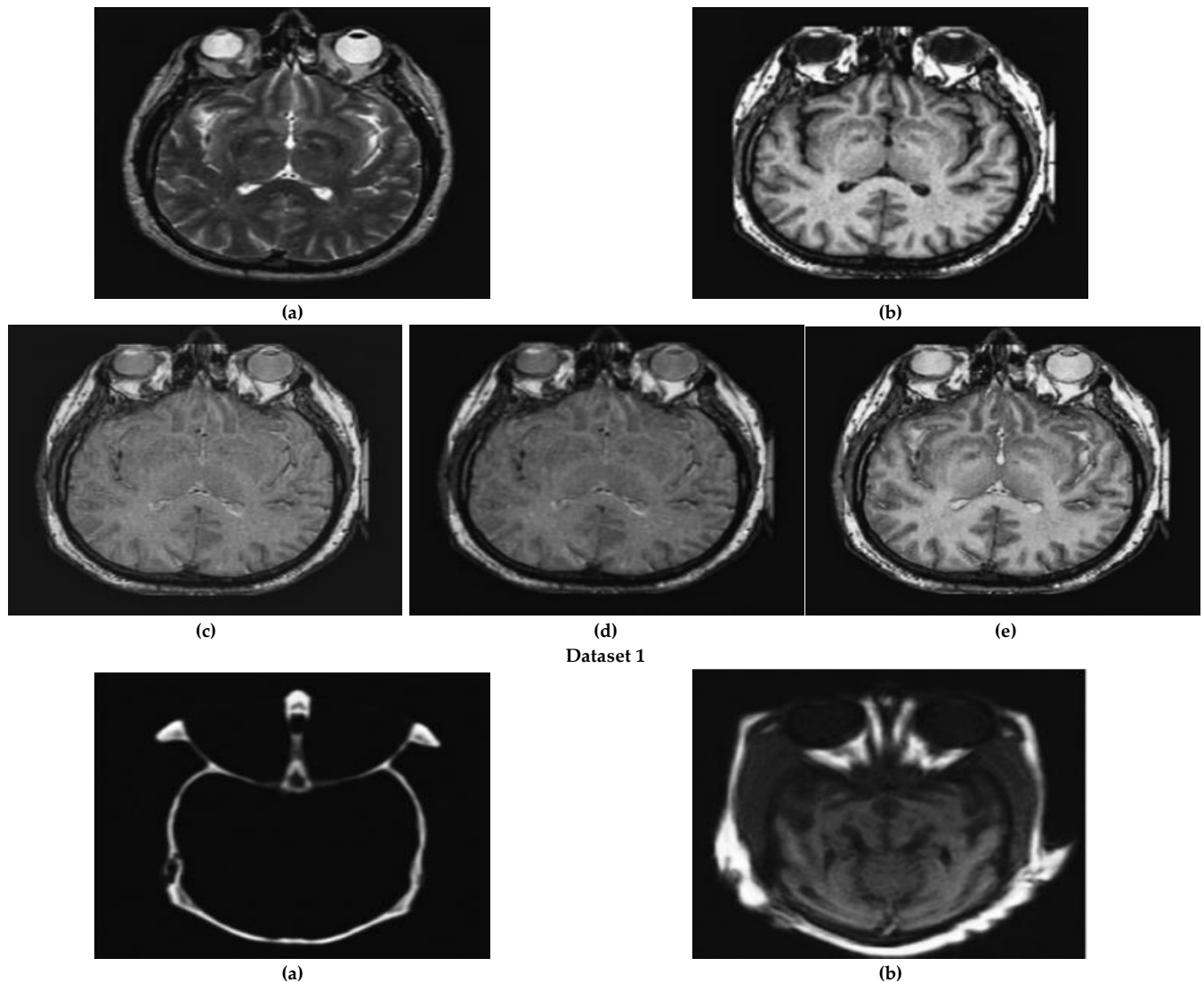


Fig. 3 IR and VI-images [16]

4. Results and Discussion

For objective evaluation, the metrics PSNR, SSIM, and MI were used. PSNR quantifies the noise reduction, SSIM evaluates structural similarity, and MI assesses the amount of shared information between images. Higher values in these metrics correlate with improved image quality. Fused images were generated using both the proposed method, PCNN, and DWT across four datasets, including medical and infrared-visible image pairs. The results (shown in Tables 1 and 2) demonstrate that the proposed method consistently surpasses both reference techniques.



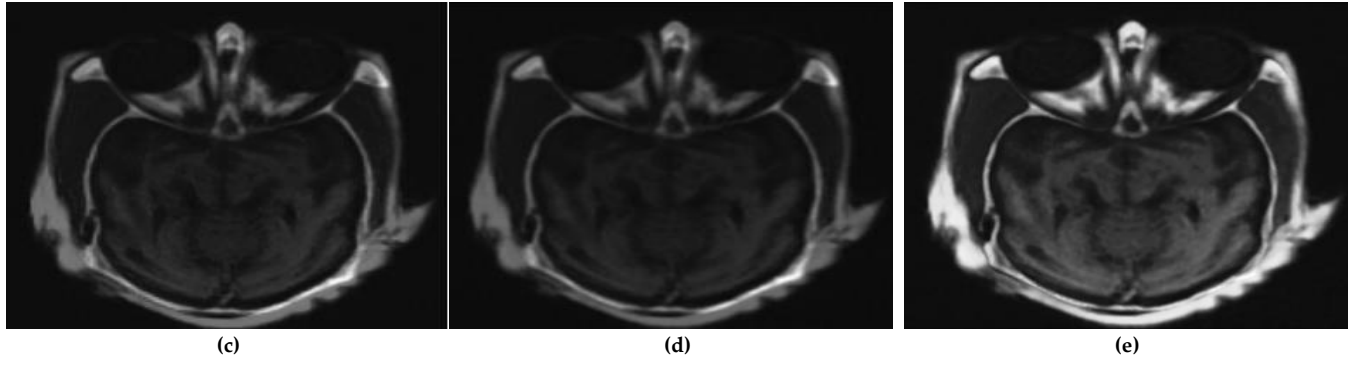


Fig. 4 Visual quality comparison on medical images

Figure in the first group of experimental images, we have (a) the original CT image and (b) the original MRI image. The fused images obtained through different methods are shown as follows: (c) using the DWT method, (d) using the PCNN method, and (e) using the proposed method.

Upon observing Figure 4, it becomes apparent that Figures 4(c), generated using the DWT method, does not capture the information from an image (b) at the corresponding position exhibiting similar visual quality. Additionally, the contrast in Figure 4(d) PCNN is relatively low and may not be easily discernible to the naked eye and produces a halo side effect. In contrast, the proposed method, showcased in Figure 4(e), demonstrates improved contrast compared to other results and successfully retains all crucial visual information from images (a) and (b).

Figure 4(a) Dataset 2 represents an MR image, while Figure 4(b) represents a CT image from the second group of brain images. Fused images from Figure 4(c) to Figure 4(e) are displayed; upon examining these results, it becomes evident that DWT (Figure 4(c)) and m-PCNN (Figure 4(d)) exhibit inadequate image contrast.

Table 1. Performance comparison of different image fusion methods across metrics and medical image datasets

Modality	Metric	DWT	PCNN	Proposed
MRI/CT Image Dataset1	En	3.561	3.698	4.482
	MI	1.192	1.492	1.974
	SSIM	0.729	0.589	0.721
	PSNR	3.561	3.698	4.482
MRI/CT Image Dataset2	En	2.332	1.998	3.125
	MI	1.455	1.786	1.983
	SSIM	0.651	0.848	0.901
	PSNR	16.845	17.054	20.665

The proposed method integrates adaptive fusion parameters and fractional calculus, which enhances the model's ability to extract key features (such as edges and textures) while preserving crucial information from the input images. This advantage becomes apparent when comparing MI and PSNR values across datasets. While DWT and PCNN yield lower MI values, obscuring fine details, the proposed method maintains higher sensitivity to pixel information, leading to improved fusion outcomes.

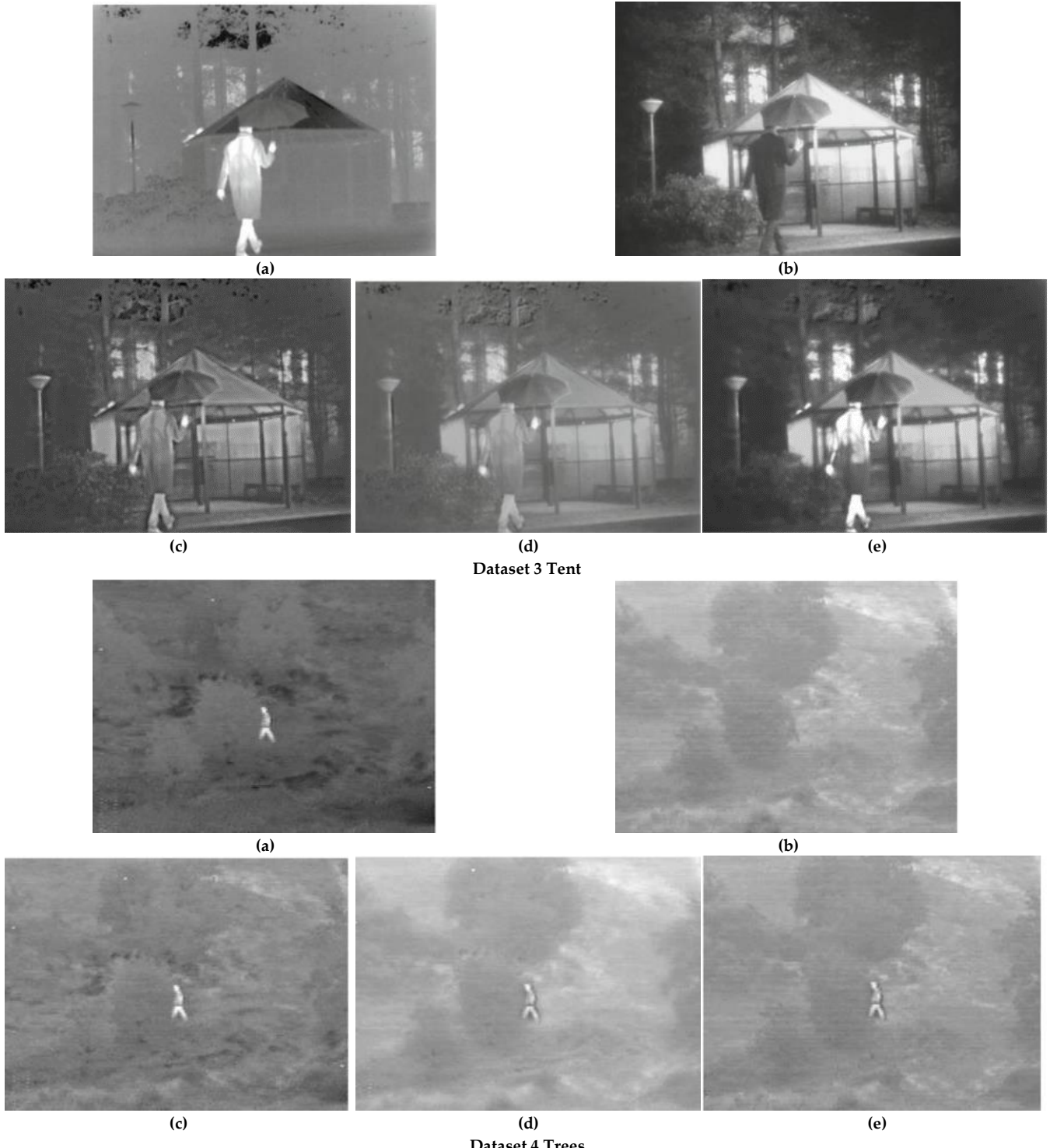


Fig. 5 Visual quality comparison on infrared and visible image

Figure 5 showcases a qualitative comparison between our method and four ablation models using five pairs of infrared and visible images from the TNO dataset. Moreover, reveals that the fused image generated by the DWT method exhibits prominent visual artifacts and artificial noise. Moreover, this method leads to a significant loss of image background information, making it unsuitable for fusing two different types of images. On the other hand, the fused image obtained by the CNN method appears more natural, but it fails to extract certain infrared details.

In contrast, our proposed method retains a greater number of infrared features in the fused image and enhances brightness to better align with the human perception system. Consequently, our results demonstrate a clear advantage over the aforementioned methods.

Table 2. Performance comparison of different image fusion methods across metrics and infrared and visible images datasets

Modality	Metric	DWT	PCNN	Proposed
IR /VI Image Dataset3	En	6.845	6.413	6.465
	MI	12.607	12.312	12.924
	SSIM	0.743	0.765	0.794
	PSNR	37.690	34.952	38.001
IR /VI Image Dataset4	En	6.512	7.028	7.412
	MI	1.483	2.056	2.175
	SSIM	0.552	0.441	0.612
	PSNR	37.514	34.698	37.3682

In Table 2, the performance of different methods is compared to ours across the four tested modalities. The results demonstrate that our method consistently outperforms the others in all cases. Furthermore, the objective metrics align with the qualitative results. Both DWT and PCNN yield lower MI values, resulting in overexposed fusions that obscure important details. In contrast, our technique generates fusion weights that exhibit a higher sensitivity to the presence of information in a pixel rather than solely relying on its absolute value.

Our method addresses key limitations of the Perona-Malik model and other state-of-the-art approaches by introducing a non-instantaneous impulsive Hilfer fractional integro-differential evolution system. This hybrid framework effectively balances noise reduction with feature preservation, making it particularly useful in applications where fine details must be preserved, such as medical imaging and surveillance.

The proposed method, based on a non-instantaneous impulsive Hilfer fractional integro-differential evolution system, shows superior performance in both medical and infrared-visible image fusion tasks. It consistently outperforms traditional methods like DWT and PCNN, offering better noise reduction and preservation of key details. This hybrid approach can serve as a competitive alternative to current deep learning models and wavelet-based techniques. Future work will focus on refining the model to enhance its applicability in other domains, such as remote sensing and real-time surveillance.

5. Conclusion

In conclusion, the proposed non-instantaneous impulsive Hilfer fractional integrodifferential evolution system has shown to be an effective method for thermal and visible image fusion. The use of fractional diffusion and impulsive fusion in a unified framework helps preserve important features such as edges and textures while fusing complementary information from the two input images. The experimental results show that the proposed method outperforms the state-of-the-art deep learning-based method in terms of both objective metrics and subjective visual quality. This method can be useful in applications such as surveillance, medical imaging, and remote sensing. Moreover, the proposed method offers a theoretical framework that provides insights into the behavior of the system and can guide the development of more efficient and robust fusion algorithms. The use of fractional calculus and non-instantaneous evolution in the proposed method allows for a more nuanced and flexible approach to image fusion, which can be beneficial in applications where the images are complex and heterogeneous.

Data Availability

The datasets used in this study are publicly available. The infrared and visible image dataset can be accessed from the TN Image Fusion Dataset at (https://figshare.com/articles/TN_Image_Fusion_Dataset/1008029). Medical images, including MRI, PET, SPECT, CT, X-ray, and MR images, were obtained from reputable sources such as Harvard Medical School's "The Whole Brain Atlas" at (<http://www.med.harvard.edu/aanlib/home.html>) and Kaggle at (<https://www.kaggle.com>). These datasets were crucial for evaluating the effectiveness of our proposed method.

Authors' Contributions

The work presented in this paper was a collaborative effort. The conceptualization, methodology, and formal analysis were all carried out by the author(s) with substantial input. Software implementation, validation, and investigation were also performed by the author(s). The original draft was written by the author(s), with review and editing taking place in collaboration. All computational work, including visualization, data curation, and resources, was managed by the author(s). No external funding or supervision was involved in this project

Acknowledgments

The author(s) would like to acknowledge that no specific assistance or contributions were received during the research and preparation of this manuscript.

References

- [1] D. Sunderlin Shibu, and S. Suja Priyadharsini, "Multi-Scale Decomposition Based Medical Image Fusion Using Convolutional Neural Network and Sparse Representation," *Biomedical Signal Processing and Control*, vol. 69, 2021. [[CrossRef](#)] [[Google Scholar](#)] [[Publisher Link](#)]
- [2] Kunpeng Wang et al., "Multi-Modality Medical Image Fusion Using Convolutional Neural Network and Contrast Pyramid," *Sensors*, vol. 20, no. 8, 2020. [[CrossRef](#)] [[Google Scholar](#)] [[Publisher Link](#)]
- [3] Lei Wu et al., "Multi-Band Remote Sensing Image Fusion Based on Collaborative Representation," *Information Fusion*, vol. 90, pp. 23-35, 2023. [[CrossRef](#)] [[Google Scholar](#)] [[Publisher Link](#)]
- [4] Jameel Ahmed Bhutto et al., "CT and MRI Medical Image Fusion Using Noise-Removal and Contrast Enhancement Scheme with Convolutional Neural Network," *Entropy*, vol. 24, no. 3, 2022. [[CrossRef](#)] [[Google Scholar](#)] [[Publisher Link](#)]
- [5] Hao Zhang et al., "Image Fusion Meets Deep Learning: A Survey and Perspective," *Information Fusion*, vol. 76, pp. 323-336, 2021. [[CrossRef](#)] [[Google Scholar](#)] [[Publisher Link](#)]
- [6] J. Sliz, and J. Mikulka, "Advanced Image Segmentation Methods Using Partial Differential Equations: A Concise Comparison," *Progress in Electromagnetic Research Symposium (PIERS)*, Shanghai, China, pp. 1809-1812, 2016. [[CrossRef](#)] [[Google Scholar](#)] [[Publisher Link](#)]
- [7] Wei Tang et al., "MATR: Multimodal Medical Image Fusion via Multiscale Adaptive Transformer," *IEEE Transactions on Image Processing*, vol. 31, pp. 5134-5149, 2022. [[CrossRef](#)] [[Google Scholar](#)] [[Publisher Link](#)]
- [8] K. Vanitha, D. Satyanarayana, and M.N.G. Prasad, "Multi-Modal Medical Image Fusion Algorithm Based on Spatial Frequency Motivated PA-PCNN in the NSST Domain," *Current Medical Imaging*, vol. 17, no. 5, pp. 634-643, 2021. [[CrossRef](#)] [[Google Scholar](#)] [[Publisher Link](#)]
- [9] Han Xu, and Jiayi Ma, "EMFusion: An Unsupervised Enhanced Medical Image Fusion Network," *Information Fusion*, vol. 76, pp. 177-186, 2021. [[CrossRef](#)] [[Google Scholar](#)] [[Publisher Link](#)]
- [10] P. Perona, and J. Malik, "Scale-Space and Edge Detection Using Anisotropic Diffusion," *IEEE Transactions on Pattern Analysis and Machine Intelligence*, vol. 12, no. 7, pp. 629-639, 1990. [[CrossRef](#)] [[Google Scholar](#)] [[Publisher Link](#)]
- [11] Leonid I. Rudin, Stanley Osher, and Emad Fatemi, "Nonlinear Total Variation Based Noise Removal Algorithms," *Physica D: Nonlinear Phenomena*, vol. 60, no. 1-4, pp. 259-268, 1992. [[CrossRef](#)] [[Google Scholar](#)] [[Publisher Link](#)]

- [12] Rafael C. Gonzalez, Richard E. Woods, and Steven L. Eddins, *Digital Image Processing Using MATLAB*, Tata McGraw-Hill, 2010. [[Google Scholar](#)] [[Publisher Link](#)]
- [13] Y.L. You, and M. Kaveh, "Fourth-Order Partial Differential Equation 0s for Noise Removal," *IEEE Transactions on Image Processing*, vol. 9, no. 10, pp. 1723-1730, 2000. [[CrossRef](#)] [[Google Scholar](#)] [[Publisher Link](#)]
- [14] Gargi Trivedi, and Rajesh Sanghvi, "Infrared and Visible Image Fusion Using Multi-scale Decomposition and Partial Differential Equations", *International Journal of Applied and Computational Mathematics*, vol. 10, 2024. [[CrossRef](#)] [[Google Scholar](#)] [[Publisher Link](#)]
- [15] Keith A. Johnson, and J. Alex Becker, The Whole Brain Atlas. [Online]. Available: <https://www.med.harvard.edu/aanlib/home.html>
- [16] Alexander Toet, "The TNO Multiband Image Data Collection," *Data in Brief*, vol. 15, pp. 249-251, 2017. [[CrossRef](#)] [[Google Scholar](#)] [[Publisher Link](#)]